APCC
APEC CLIMATE CENTER

# RESEARCH REPORT

APCC
APEC CLIMATE CENTER

# PREFACE

It is our pleasure to present this report on the APEC Climate Center (APCC)'s research activities in 2013, which has been a very productive year for our Center.

APCC has expanded its research scope, in response to regional societal and scientific needs. While building expertise in climate prediction remains a priority, we are extending our reach to include policy-relevant climate applications and value-added climate information products.

APCC has accelerated efforts to better our service to the region. As one of the main services provided by APCC, the MME 3-month prediction information has been productively applied by scientists in developing countries that are unable to produce their own prediction information. Furthermore, in order to better prepare for climate-related hazards in a timely manner, APCC launched its 6-month MME prediction service in September 2013. We also began to release forecasts of the Boreal Summer Intraseasonal Oscillation (BSISO), starting from July 2013, as the world's first operational BSISO forecast service. Our researchers also achieved great success in publishing their papers in noted academic journals. Dr. Ok-Yeon Kim, for example, published a paper in *Climate Dynamics* and her research was later selected as one of the Research Highlights by another distinguished journal, *Nature Climate Change*. The following research report provides more information about our research outcomes from 2013.

We will continue to promote the best use of our research outcomes in various scientific and application areas. Our successes and achievements would not have been possible without the support of our valued partners. In this regard, I extend my thanks to you and I hope you enjoy this 2013 Research Report.

Chin-Seung Chung
Director, APEC Climate Center

# CONTENTS

APCC

RESEARCH REPORT 2013-02

# Long-lead Station-scale Prediction of a Hydrological Drought in South Korea Based on Bivariate Downscaling

Dr. Soo-Jin Sohn | Climate Prediction Team

**ABSTRACT**

Capturing climatic variation from boreal winter to spring (December to May) is essential for the proper prediction of drought in South Korea. This study uses observed datasets and multi-model ensemble (MME) hindcast experiments (1983/84-2005/06) archived at the APEC Climate Center (APCC) to investigate the variability and predictability of the South Korean climate during the period December-May. It focuses on the leading modes of winter-to-spring variability over South Korea, which are identified based on multivariate empirical orthogonal function (EOF) analysis of the 6-month accumulated precipitation and surface air temperature. The first two leading climate modes, accounting for about 80% of total variance, are characterized by national-scale precipitation and temperature anomalies covering an entire region over South Korea.

A perfect empirical model was developed to reveal atmospheric dynamic linkage (based on the observed datasets), and be used as a standard reference to recognize its physically potential predictability. The potential of using a hybrid dynamical-statistical method for a 6 month-lead (with November as the initial condition) drought prediction was also investigated. Nine one-tier climate models were statistically downscaled for predicting the standardized precipitation evapotranspiration index (SPEI) over 60 stations in South Korea. This bivariate and pattern-based downscaling was employed for both precipitation and temperature, to maintain a physically coherent relation between these factors, and a spatial coherence over the 60 station locations. This study has developed a new downscaling method using a variant of canonical correlation analysis (CCA). Precipitation and temperature predictions, based on dynamically better-predicted sea level pressure (SLP) and 500hPa geopotential height (Z500) were substantially improved in the downscaled MME (DMME). The limitations of the hybrid dynamical-statistical model, and possible causes for these in the current framework of dynamical climate prediction were also discussed for further improvement.

Overall, DMME gives reasonably skillful long-lead forecasts of SPEI for the period winter-spring, compared to raw MME. Our results could lead to more reliable climatic extreme predictions for policymakers and stakeholders in the water management sector, and for the mitigation of problems related to climate change.

# 1. INTRODUCTION

The multimodel ensemble (MME) approach has been designed as an effective way for quantifying forecast uncertainties due to model formulation (e.g. model parameterization of unresolved sub-grid scale process) (Krishnamurti et al., 1999, 2000; Doblas-Reyes et al., 2000; Shukla et al., 2000; Palmer et al., 2000), and is

recognized as a valuable tool for improving dynamical weather and climate forecasts. The prediction skills of MMEs are generally better than those of single models from either two-tier (Krishnamurti et al., 1999, 2000; Shukla et al., 2000; Palmer et al., 2000; Barnston et al., 2003) or one-tier prediction systems (Hagedorn et al., 2005; Doblas-Reyes et al., 2005; Yun et al., 2005). For this reason, MMEs are used by several major operational centers for seasonal climate prediction (Palmer et al., 2004; Climate Test Bed, 2006; Lee et al., 2009). Moreover, a number of efforts have been made to intercompare models (Sohn et al., 2011), and to synthesize them with optimal MME methods using either linear (Krishnamurti et al., 2000; Yun et al., 2003; Kug et al., 2008), or nonlinear approaches (Acharya et al., 2013).

Despite the remarkable advances made in relation to the advent of MMEs in dynamical seasonal prediction, there are still relative deficiencies and limitations in predicting long-term climate variability and extreme phenomena on local and regional scales, particularly over the extratropics. This may be predominantly due to the inherent low predictability over mid-to-high latitudes, coarsely resolved model output, initial value problem and associated chaotic dynamics, and forecast lead-time and error growth. For instance, predicting summer mean precipitation over the Asian summer monsoon region, even with a 1 month lead, remains challenging for climate models (Wang et al., 2007, 2008a, 2008b, 2009, Kug et al., 2008; Lee et al., 2010, 2011). Hence, a number of approaches to bridge the gap between dynamical climate models and regional information (i.e. statistical post processing or downscaling) have been applied to appropriately predict long-lead, small-scale climate variability and extremes (Kang et al., 2007, 2009; Min et al., 2011b; Sohn et al., 2013a, 2013b; Tung et al., 2013). A downscaling technique has also been used as a diagnostic tool to verify the performance of climate models on a regional scale (Busuioc et al., 1999). In addition, efforts have been made to extend a forecast lead time of up to 6 months over mid-to-high latitudes, and to improve extended forecast skills (Sohn et al., 2012, 2013a).

Boreal winter brings less precipitation than other seasons in South Korea, making the country susceptible to spring droughts (Min et al., 2011a). The amount of winter precipitation is, therefore, an important factor in determining springtime drought

conditions, which can greatly impact agriculture practices such as irrigation and seeding. In addition, a 6-month period represents the typical time scale for precipitation deficits to affect ground water for hydrological management (McKee et al., 1993). Capturing climatic variation from winter to spring (December to May) is therefore essential for properly predicting drought in South Korea.

Droughts in South Korea and East Asia are associated with anomalous large-scale atmospheric circulation in the northern hemisphere, rather than local factors (Park and Schubert, 1997; Kim et al., 2005). For example, an extremely severe drought in the spring of 2001 was associated with an abnormally strong high-pressure system in the center of the Eurasian continent (Lee et al., 2001). Some major droughts in the midlatitudes of the northern hemisphere are attributed to atmospheric teleconnections related to tropical sea surface temperature (SST) variability (Barlow et al., 2002; Hoerling and Kumar, 2003; Schubert et al., 2007). In addition, droughts in East Asia are closely related to droughts in Korea (Min et al., 2003). However, climatic variation and extreme drought events occurring from winter to spring in South Korea in relation to local-to-global teleconnections has been not yet been clearly revealed. Sohn et al. (2013a) showed that surface air temperature and precipitation during the 6-month period have high interannual variations, and are positively correlated with each other (see also Figure 1), which implies that consideration of both the effect of temperature and precipitation variability on extreme drought is necessary to properly define long-term hydrological variations over South Korea. However, the study did not downscale temperature and precipitation independently, and information pertaining to large-scale circulations was used separately, which makes it possible that there is no physically coherent relation between downscaled temperature and precipitation, even under the same climate conditions such as large-scale circulation.

It is therefore considered essential to maintain a physically coherent relation between temperature and precipitation. However, most of MME-based downscaling methods have focused on just a single variable, e.g. seasonal mean precipitation (Kang et al., 2007, 2009; Sohn et al., 2013a, 2013b). In addition, previous downscaling methods have been based on point-wise regression, where the predictor for one

station may be different from another (Kang et al., 2009; Sohn et al., 2013a, 2013b), which means that spatial coherence under the same background climate can be disregarded. Therefore, in this study we seek to develop a reliable long-lead, district-level, MME-based prediction system for droughts, using a statistically bivariate and pattern-based downscaling method. The novelty of this approach is that it delivers a more physically-meaningful statistical downscaling method compared to previous methods, and combines the merits of bivariate and pattern-based downscaling for both precipitation and temperature.

This paper is organized as follows: Section 2 describes the data and methodology used; Section 3 presents the results for a perfect empirical model, a hybrid dynamical-statistical model, and extreme drought predictions across South Korea. Section 4 presents a summary and a discussion of the results.

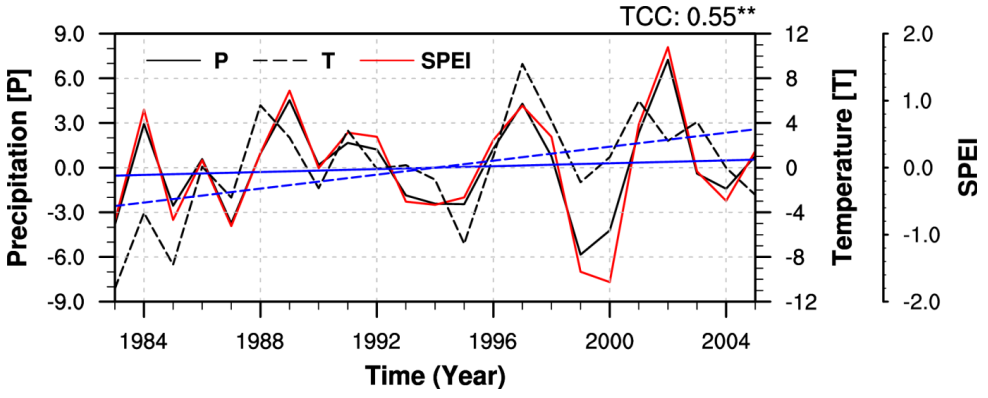


**Figure 1** Time series of observed December-May anomalous precipitation (solid black line); surface air temperature (black-dashed line); and the standardized precipitation evapotranspiration index (SPEI) (solid red line) during the period 1983/1984-2005/2006, averaged over 60 station locations in South Korea. The correlation between the former two time series exceeds the 5% significance level, and its value is given in the upper right corner. Straight solid and dashed lines (in blue) show the linear trend of precipitation and temperature measurements, respectively (as in Sohn et al. (2013a) with an extension up to 2005/2006.)

# 2. DATA AND METHODOLOGY

## 2.1 Data

In this study, the prediction period of interest is for six months (December-May). Table 1 lists acronyms of the institutions and models mentioned in the text, and Table 2 presents a brief summary of model specifications for the nine one-tier models, and the current status of retrospective forecasts. APCC models have generated ensemble retrospective forecasts for the approximately common years of 1983/84-2005/06. Each model has a different forecast length and ensemble size (Table 2), but all models were integrated on 1 November for the boreal winter and spring seasons. Flux correction is not applied to any coupled model.

**Table 1** Acronyms and names of institutions and models used

| Acronym | Full names |
|---|---|
| APCC | Asia-Pacific Economic Cooperation Climate Center |
| BOM | Bureau of Meteorology |
| CCCma | Canadian Center for Climate Modelling and Analysis |
| CCSM | Community Climate System Model |
| CFS | Climate Forecast System |
| GMAO | Global Modeling and Assimilation Office |
| MSC | Meteorological Service of Canada |
| NASA | National Aeronautics and Space Administration |
| NCEP | National Center for Environmental Prediction |
| PNU | Pusan National University |
| POAMA | Predictive Ocean-Atmosphere Model for Australia |
| SNU | Seoul National University |
| UH | University of Hawaii |

The observational datasets used in this study are taken from the reanalysis products of the National centers for Environmental Prediction-National Center for Atmospheric Research (NCEP-NCAR) (Kalnay et al., 1996), and cover the same period as the observational dataset in this study. The pool of predictors comprises atmospheric

variables such as sea level pressure (SLP), 2 m air temperature (T2M), 500hPa geopotential height (Z500), 850hPa temperature (T850), 850 and 200hPa winds (UV850 and UV200), and the oceanic variable of SST (the latter is included because of the potential link between tropical SST and drought events in the midlatitudes (see Introduction)). Based on the physical relation between the observed standardized precipitation evapotranspiration index (SPEI; Vicente-Serrano et al., 2010), and the observed large-scale circulation patterns, the predictor domain of 60°E-160°W, 0-80°N is chosen (see in Figure 2b).

Additional baseline reference surface air temperature and precipitation data were obtained from 60 stations in South Korea, (as shown in Figure 2: source: http://www.kma.go.kr/weather/observation/past_table.jsp), and were used to calibrate and validate temperature and precipitation predictions at the target locations (for more information, see Sohn et al. (2013b)).

Eight climate indices of the Northern hemisphere teleconnection patterns, such as the North Atlantic Oscillation (NAO), East Atlantic Pattern (EA), West Pacific Pattern (WP), East Pacific /North Pacific Pattern (EP/NP), Pacific-North American Pattern (PNA), East Atlantic / West Russian Pattern (EA/WR), Scandinavia Pattern (SCA), Polar/Eurasia Pattern (POL), were obtained from http://www.cpc.ncep.noaa.gov/data/teledoc/telecontents.shtml. Prominent teleconnection patterns are identified in the Northern Hemisphere extratropics throughout the year, and all these patterns have previously appeared in meteorological literature (Barnston and Livezey, 1987). These patterns and indices were identified by orthogonally rotated principal component analysis (RPCA; Barnston and Livezey (1987)) of the Northern Hemisphere monthly mean, at 500-hPa geopotential height.

**Table 2** Description of the nine climate models used in this study.

| Country | Institute | Model | AGCM/resolution | OGCM/resolution | Ensemble Member | Period | Reference |
|---|---|---|---|---|---|---|---|
| Australia | BOM | POAMA 2.4 | BAMv3.0d/T47L17 | ACOM2/0.5-1.5°lat x 2°lon L25 | 10 | 1960-2010 | Cottrill et al. (2013) |
| Canada | MSC | CCCma CGCM3[1)] | AGCM3/T63L31 | OGCM4 (1.41°lon x 0.94°lat L40) | 10 | 1981-2010 | Merryfield et al. (2013) |
| | MSC | CCCma CGCM4[2)] | AGCM4/T63L31 | | 10 | 1981-2010 | |
| Korea | APCC | CCSM3 | CAM3/T85L26 | POP1.3/Gxlv3_L40 | 5 | 1983-2011 | Jeong et al. (2008) |
| | PNU | PNU | CCM3/T42L18 | MOM3/0.7~2.8 lat L29 | 10 | 1979-2009 | Sun and Ahn (2011) |
| | SNU | SNU | SNU/T42L21 | MOM2.2/L2lat x 1°lon L32 | 6 | 1981-2011 | Ham and Kang (2010) |
| USA | NASA | GMAO | GEOS-5/288x181L 72 | MOM4/720 x 410 L40 | 9 | 1982-2012 | Ham et al. (2012) |
| | NCEP | CFSv2 | GFS/T126L64 | MOM4/OMlat x 1°lon L40 | 20 | 1982-2009 | Saha et al. (2010) |
| | UH | UH | ECHAM4/T31L19 | UH Ocean/1°lat x 2°lon L2 | 10 | 1982-2005 | Fu and Wang (2004) |

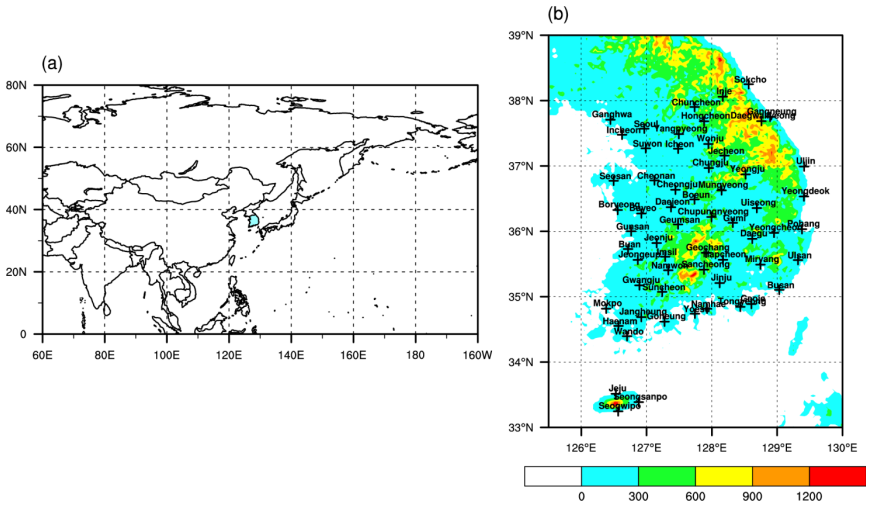


**Figure 2** (a) Predictor domain for South Korea considered in this study indicated by shading; and (b) topographic map (shaded; units: m) with locations of 60 stations (marked with crosses). See text for details.

1) http://www.ec.gc.ca/ccmac-cccma/default.asp?lang=En&n=1299529F-1

2) http://www.ec.gc.ca/ccmac-cccma/default.asp?lang=En&n=3701CEFE-1

## 2.2 Methodology

Local surface air temperature and precipitation forecasts at 60 stations in South Korea are produced using a perfect empirical model and a dynamical-statistical method, which are a bivariate and pattern-based statistical downscaling. The downscaling method was newly developed on the basis of a variant of canonical correlation analysis (CCA), which finds the optimum linear combination of two multidimensional vectors (predictands and predictors) and selects pairs of patterns of spatial- and temporal-dependent variables to optimally correlate their coefficient time series (Barnett and Preisendorfer, 1987). The CCA could also be used to understand large-/regional-scale mechanisms controlling climate variability across the analyzed area, in particular with respect to extreme events (Busuioc et al., 2008). The pattern-based regression model makes full use of CCA as a transfer function [ref. Eq. (A14)].

This prediction methodology is an improved version of that of Barnett and Preisendorfer (1987; hereafter known as the BJ method), who suggested that filtering the data for each field by projecting it onto a subset of the EOFs of that field can make CCA less susceptible to sampling fluctuations due to a short time series. CCA defines coordinate systems that optimally describe the cross covariance between two different datasets [ref. Eqs. (A3)-(A7)]. The major difference between "classical" CCA and BP is also summarized in Bretherton et al. (1992). The novelty of the method developed in this study, which is not used in the BJ method, is the compression of data for data filtering via the multivariate EOF (the spatial fields of predictand data from two different variables, such as precipitation and surface air temperature), are concatenated. The composite predictand set ($T$) can be defined by:

$$T(x', \mathrm{t}) = \begin{cases} P(t,\eta) & x' = 1,2,\ \cdots, m; \quad \eta = 1,2,\ \cdots, m \\ T(t,\eta) & x' = m+1,2,\ \cdots, 2m; \quad \eta = 1,2,\ \cdots, m \end{cases}, \qquad (1)$$

where t = 1, 2, ⋯, n and $x' = 1, 2, \cdots, 2m = q$

Another key feature of this method is that instead of using conventional EOF analysis, multivariate EOF is employed to keep the physically coherent relation between temperature and precipitation. For the predictor, univariate EOF with SLP,

Z500, T2M, T850, etc. is performed to filter the data, as both EOF, and multivariate EOF analyses yield a more dynamically balanced view of the target variables (Mu et al., 2004). Multivariate EOF analysis extends the processing of the conventional EOF by considering both spatial and inter-variable coherence. This often leads to greater physical insight into the interactive processes within a complex system, such as the ocean-atmosphere system (see Wang (1992) for more details). The rest of the prediction methodology used is the same as that of Barnett and Preisendorfer (1987), and further described in the Appendix.

A perfect empirical model was developed to reveal atmospheric dynamic linkage based on the observed datasets, and for use as a standard reference to recognize its physically potential predictability. In other words, when a dynamical model perfectly predicts the observed atmospheric large-circulation pattern (as predictor), the limit of predictability is inferred from the perfect empirical model. A hybrid dynamical-statistical model is the model output statistics (MOS; Wilks, 1995)-typed downscaling scheme using model large-scale variables to predict local temperature and precipitation. Single-model climate ensembles are calibrated using the CCA between observed local variables and model large-scale variables, and the statistically downscaled single models are then combined with equal weights to create a downscaled MME (DMME). Furthermore, for reliability enhancement, appropriate inflation was applied to correct the small variance of MME and regression-based downscaled outputs (Sohn et al., 2013a, 2013b). The method simply rescales the variance of predicted rainfall and temperature to that based on their respective climate records (see the Appendix for more details).

All the procedures for both calibration and combination are carried out in the cross-validated mode (Michaelsen, 1987), which is used to estimate the model's true forecast skill. Leave-one-out cross-validation (LOOCV), one of common types of cross-validation, is also employed. This uses a single observation from the original sample as validation data, and the remaining observations as training data. This is repeated so that each observation in the sample is used once as the validation data. This is the same as K-fold cross-validation; K being equal to the number of observations in the original sampling. All procedures for both the perfect empirical

model, and a hybrid dynamical-statistical model, were carried out in the cross-validated mode. The process (such as the use of data compression, calibration using CCA, combination, and inflation) used to construct (train) the forecast model, was repeated 23 times, sequentially omitting a single data map pair (i.e. predictor and predictand) each time (see Barnett and Preisendorfer (1987) for further information).

The final station-scale temperature and precipitation predictions were then used to produce drought forecasts on the basis of SPEI, which involves computing the accumulated deficit or surplus of the climatic water balance (the difference between precipitation and potential evapotranspiration) and adjusting this to a log-logistic probability distribution. Following Vicente-Serrano et al. (2010), potential evapotranspiration was calculated empirically from air temperature. Because the ultimate goal was to predict 6 month SPEI (hereafter referred to as SPEI6), we only considered 6 months of accumulated precipitation and temperature data during December to May as the input for SPEI calculations. Temporal correlation (Barnston, 1994), and the linear error in probability space (Potts et al., 1996), which measures the error in the probability space rather than in the real measurement space, were used to assess the skill of extreme predictions.

## 3. RESULTS of RESEARCH

### 3.1 Dominant modes of winter-to-spring climate variability in South Korea

In order to capture the dominant modes of winter-to-spring climate variability in South Korea, multivariate EOF analysis is employed using temperature and precipitation. Figure 3 shows the spatial patterns and time coefficients of the five leading modes of multivariate analysis for the observed winter-to-spring precipitation and temperature during the 23 year period from 1983/84-2005/26. It is found that the first two leading modes, which have the same sign over South Korea, explain 81% of the total variance, which suggests that most total temperature and precipitation variances may be induced by the same large-scale system. In addition, three other

modes explain a sum of 8.9% of the total variance (see Figure 3), and each mode has a relatively more localized structure compared to the first two leading modes. We therefore focus on the first two leading modes of winter-to-spring time variability over South Korea.

The leading climate mode is characterized by national-scale precipitation and temperature anomalies covering a whole region, which are in phase with same sign. During the peak of El Niño in boreal winter and the ensuing spring, the climate in East Asia tends to be warmer and wetter than usual (Wang et al., 2000), which implies that changes in precipitation have a relationship with those of temperature. The second mode is associated with out-of-phase fluctuations between temperature and precipitation over all the locations in South Korea. In general, on a seasonal basis, a negative correlation between temperature and precipitation can be expected. Soil moisture controls the energy balance between the surface and atmosphere by the contrast between latent and sensible heat, and the fluctuations of temperature and moisture are controlled by the feedback between precipitation and soil moisture (Schär et al., 1999). However, the rainfall deficit brings a deficit in soil moisture, and consequently extreme heat waves and severe droughts.

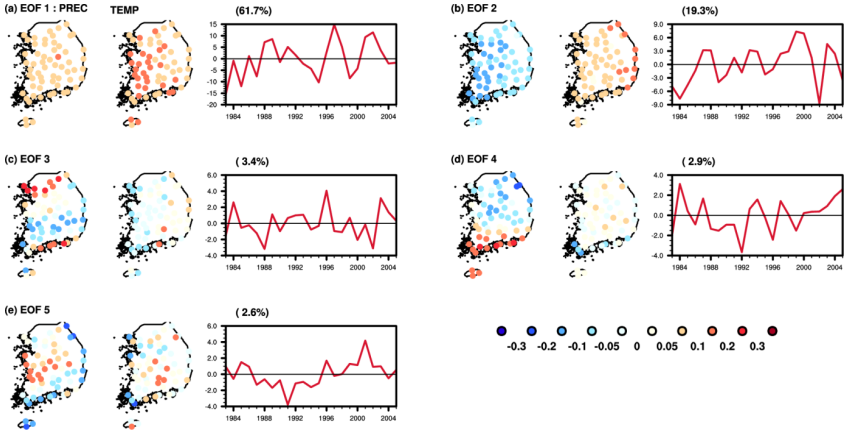


**Figure 3** (a) Multivariate empirical orthogonal function (EOF) patterns and time coefficients of the observed December to May anomalous precipitation and surface air temperatures in South Korea over 23 years from 1983/1984-2005/2006 for the: (a) first, (b) second, (c) third, (d) fourth, and (e) fifth modes. The respective panels consist of spatial patterns of precipitation (left column) and surface air temperature (middle column) as well as principal component (PC) time series (right column).

As mentioned in the Introduction, it is considered likely that winter-to-spring droughts in South Korean are influenced by certain major modes of climate variability. To access the link between the South Korean climate and other climate modes using the observational record, correlation coefficients between the first two PCs from the multivariate EOF analysis, and the NAO, EA, WP, EP/NP, PNA, EA/WR, SCA, POL, Artic Oscillation (AO; Thompson and Wallace, 2000), Siberian high (SH), and Nino3 are given in Table 3. The Siberian high index is defined as the SLP anomaly averaged over the area 80-120°E, 40-60°N (see Jhun and Lee (2004)). Finally, the AO index is defined as the first principal component of the SLP to the north of 20°N.

**Table 3** Correlation coefficients between the first and second PC time series and various climate indices computed using accumulated values within the whole period December to May from 1983/84-2005/2006, based on observations. Values exceeding the 1% significance level are marked by double asterisks, and those exceeding the 5% significance level by single asterisks.

| Indices | PC 1 | PC 2 |
|---|---|---|
| NAO | 0.07 | 0.33 |
| EA | 0.43* | 0.20 |
| WP | 0.62** | 0.16 |
| EP/NP | 0.32 | 0.07 |
| PNA | -0.38 | 0.09 |
| EA/WR | 0.71** | -0.03 |
| SCA | -0.36 | -0.44* |
| POL | 0.21 | -0.43* |
| AO | 0.44* | 0.16 |
| SH | -0.59** | -0.43* |
| Nino3 | 0.44* | 0.13 |

The correlation analysis shows that these two modes are not simultaneously associated with the NAO, but it is known that the winter and spring NAO has an impact on the summertime atmospheric circulation over East Asia (Ogi et al., 2003). It can be seen, however, that the first mode is closely related to the EA, WP, EA/WR, and AO patterns for the winter-to-spring period. This suggests that during the period, the fluctuation of temperature and precipitation in South Korea may be caused by the phases of patterns over the East Atlantic/Western Russian or over the West

Pacific. The AO index is also correlated with the leading PC, which implies that a positive AO is likely to be associated with warmer and wetter than usual conditions in South Korea. The SCA and POL patterns are found to be associated with the occurrence of the second climate mode, but are unrelated to the first mode. In addition, both leading climate modes are related to the strength of the Siberian high, as evidenced by the high correlation between the SH index and the two leading PCs, and SH variability is highly related to each variability in precipitation and temperature, respectively (Gong and Ho, 2002).

## 3.2 Development of a dynamical-statistical prediction model for the winter-to-spring climate

### 3.2.1 A perfect model based on observed linkage

Correlation analysis was used to reveal atmospheric or ocean dynamic linkage based on the observed data, and the linkage observed provided a robust basis for the choice of predictor and its range in predicted fields. From the correlation analysis between the observed station SPEI and the observed SLP, Z500, T850, U850, V850, U200, V200, T2M, SST, and precipitation, the predictor domain of 60-200°E, 0-80°N is commonly chosen (see the result in Figure 4). Previous studies by Kug et al. (2008), Kang et al. (2009), and Sohn et al. (2013a, 2013b) have searched the predictor domain per each station using global scanning. In this case, physically unlinked region or domain can be randomly selected just based on artificially statistical result, or one station can have different predictor domain from another station. To avoid the problem, we selected the prediction domain using SPEI, which is calculated by temperature and precipitation averaged over 60 station locations in South Korea (see Figure 1 for the time series). As a result, the domain in the vicinity of Korea was selected, which is large enough to cover the large-scale circulation in the Northern Hemisphere (relevant to result to Table 3), and the occurrence of drought in Korea is seen to be highly correlated with those over East Asia (Min et al., 2003; see also Introduction).

Most atmospheric circulations have an impact on the occurrence of hydrological extreme events (Figure 4a-h, j). However, the impact of local oceanic circulations on local scale extreme events are not shown to be significant, at a 90% confidence level (Figure 4i), although there is a remote oceanic impact from the Indo-Pacific (see Introduction).

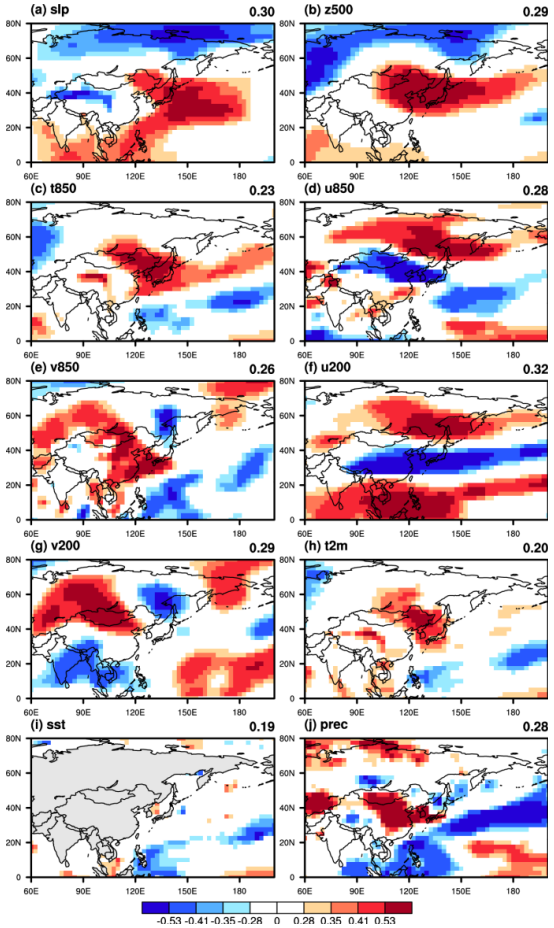


**Figure 4** Temporal correlation coefficients (TCCs) of observed December to May anomalous potential predictors from: (a) mean sea-level pressure (SLP; units: hPa); (b) 500hPa geopotential height (Z500; m); (c) 850hPa temperature (T850; °C); (d) 850hPa meridional wind component (U850; m/s); (e) zonal wind component (V850; m/s); (f) 200hPa meridional wind component (U200; m/s); (g) 200hPa zonal wind component (V200; m/s); (h) 2m temperature (T2M; °C); (i) sea surface temperature (SST; °C); and (j) precipitation (PREC; mm/day) with SPEI during the 1983/1984 to 2005/2006 period, over the predictor domain. Values with absolute magnitudes of 0.53, 0.41, 0.35, and 0.28 represent the 99%, 95%, 90%, and 80% confidence intervals, respectively. The area-averages of absolute values over the domain are provided in the upper right of each panel.

Figure 5 shows the patterns of the first CCA pairs for observed station precipitation and temperature, as well as the observed SLP (for the second mode, Figure A1). The canonical correlation coefficient between the time series, associated with the patterns of the predictand (precipitation and temperature; Figure 5a) and predictor (SLP; Figure 5b) is 0.86, and the corresponding explained variance are 57% and 18%, respectively. This indicates that the first leading mode explains a very similar pattern to the first mode of the multivariate EOF analysis based on precipitation and temperature (see Figure 3). The climate mode is characterized by national-scale precipitation and temperature anomalies, covering a whole region, which are in phase with the same sign, implying that changes in precipitation have a relationship with those of temperature. The leading canonical mode represents a reasonable dynamic link: for example, a western high and eastern low pressure system centered over respective Siberia and Aleutian regions,= is favorable for the occurrence of westerly or northwesterly low-level bringing colder and drier air over the Korean Peninsula from the Arctic. It is known that South Korea is affected by the formation of the continental high pressure system in Eurasia during boreal winter, and is affected by the Siberian high, and by the migratory high stemming from the continental high during spring time. Using CCA, it is also found that the dominant spatial pattern of interannual variability of winter-to-spring precipitation and temperature is associated with a seesaw structure between the southern and northern parts of East Asia. This dynamic linkage will be used in a dynamical-statistical model further in the paper (shown in subsection 3.2.3).

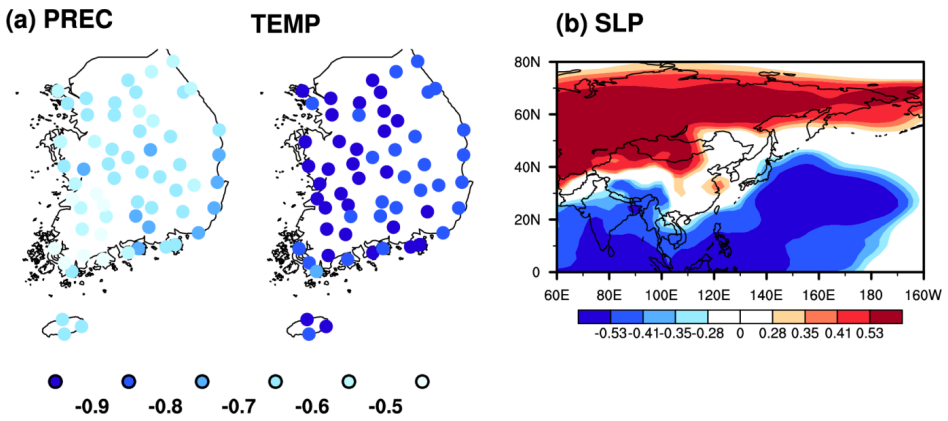


**Figure 5** Canonical maps of observed December to May anomalous precipitation (left panel), and surface air temperature (middle panel), over 60 station locations in South Korea, and simultaneous SLP in the predictor window for the first mode. The canonical maps represent vectors at specific locations between the predictand (or predictor) and their respective canonical component time series. These patterns explain 57% and 18% of the total variances for predictand and predictor, respectively. The correlation between the respective amplitude time series for these patterns is 0.86. See text for further details.

The perfect empirical model was developed based on dynamic linkage (i.e. based on the CCA and using observed station data and observed large-scale variables), in order to investigate the skill of the perfect model as a reference. Figure 6 compares the temporal correlation coefficients (TCC) between the observed and the perfect empirical model's 6-month accumulated rainfall and temperature at each station location for each predictor. The values of the TCCs averaged over the 60 stations for both temperature and precipitation are given as x- and y- coordinates (in parenthesis) in Figure 6, and the "standard distance deviation" of both precipitation and temperature is also given. It is clear that the skills vary from one predictor to another. It is also noteworthy that the predictor cannot guarantee to properly predict both precipitation and temperature. The dispersion of skills over 60 stations is also comparably larger for precipitation and temperature than those from other predictors. These localized variables can be not appropriate in prediction station-scale precipitation and temperature. Even though the dispersion of skills from upper-air temperature is smaller than that from surface air temperature, 850-hPa temperature has done to make skillful precipitation forecast.

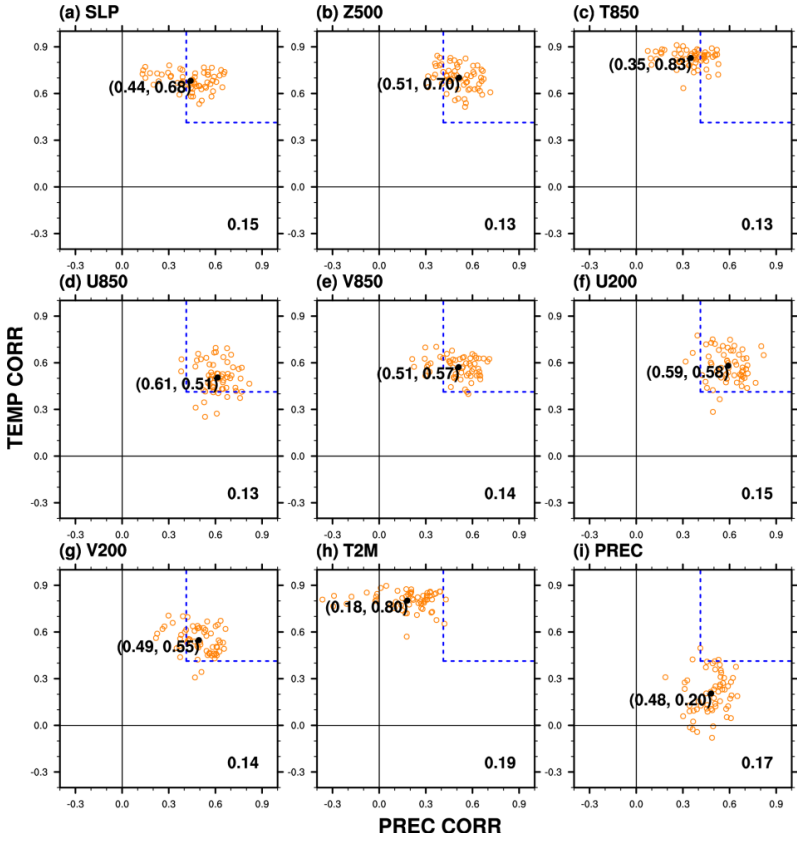


**Figure 6** Scatter plots of TCCs between the observed and predicted precipitation (x axis) and temperature (y axis), for the potential predictor of: (a) SLP, (b) Z500, (c) T850, (d) U850, (e) V850, (f) U200, (g) V200, (h) T2M, and (i) PREC. Each orange point represents the results based on perfect model predictions for one station location. The black dots denote the TCC values averaged over 60 stations in South Korea. The rectangle in the top right corner of each panel (partly surrounded by blue-dotted lines) denotes the zone exceeding the 5% significance level for both precipitation and temperature. The "standard distance deviation" of both precipitation and temperature is given at the bottom right of each panel. See text for further details.

### 3.2.2 Dynamical vs. hybrid model

Figure 7 compares the TCC between the observations and the MME average of the raw general circulation mode (GCM) prediction, and that based on DMME prediction, for 6-month accumulated rainfall and temperature at each station in DJFMAM. MME products are spatially interpolated on the 60 station locations (in a very similar way to the bias-corrected local scaling (BLS) method (Wood et al.,

2002)) for comparison between ram MME and DMME. It can be seen that the interpolated raw MME products give large errors for precipitation and temperature (Figures 7a and 7d). On the other hand, statistical downscaling for precipitation can correct a large proportion of the systematic error over South Korea, while the cross-validated temporal correlation of the DMME prediction, based on SLP as predictor, is comparable with that from the raw MME for temperature. This is evidenced by the downscaling results in Figure 7. The skill difference between raw MME and DMME based on 60-station-averaged TCC value is 0.05 for precipitation, and only 0.01 for temperature.

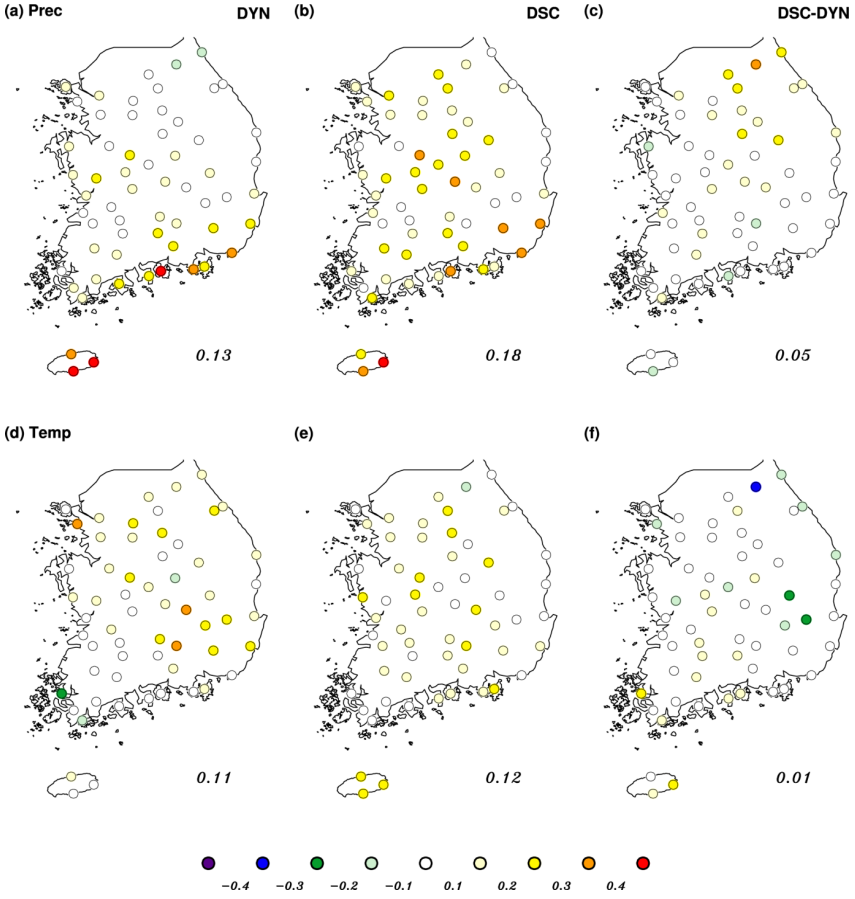


**Figure 7** TCCs between observed and predicted (a, b, c) precipitation, and (d, e, f) temperature from December to May, from (a, d) raw mutlimodel ensemble (MME), (b, e) downscaled MME (DMME), and (c, f) their difference for each station. The temporal correlation averaged over the 60 stations is given in the bottom right of each panel.

To represent the skills of precipitation and temperature forecasts for raw MME and DMME averaged over the whole South Korean region from various predictors, the forecast values are first averaged all station points. Figure 8 shows the average correlations as a function of the predictor, based on the six atmospheric circulation variables. DMME precipitation forecasts from all predictors have superior skills compared to those of the MME forecasts. However, DMME temperature forecasts show a wide range of skills compared to those of DMME precipitation, and although SLP and Z500-based results are more improved than the raw MME, DMME temperature forecasts from wind component-based predictors give a poorer correlation than those from other predictors.

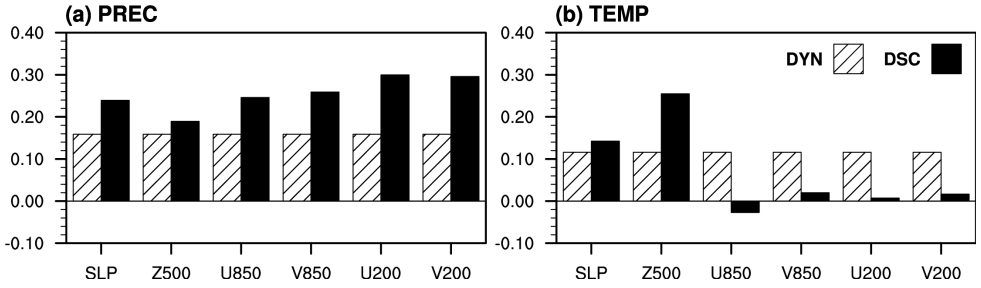


**Figure 8** TCCs between the observed and predicted: (a) precipitation, and (b) temperature from December-May during the period 1983/84 to 2003/2004, averaged over 60 stations locations in South Korea. Hatched-bars denote raw MME; solid bars denote DMME.

### 3.2.3 Limitation of hybrid model and reasons for limitation

The ability of a hybrid dynamical-statistical model in predicting precipitation and temperature variation over South Korea is related in the above subsection 3.2.2. In this subsection, the limitation of the hybrid model and its potential causes are further studied, focusing on the model's skill in reproducing fluctuations of atmospheric large-scale circulation patterns in hindcast simulations. To quantify the ability of the model to reproduce atmospheric large-scale patterns, TCCs between, and simulated patterns over, the predictor domain were computed (results are shown in Figure 9). Among the various predictors, SLP and Z500 have higher skills than the other variables (corresponding with the results in Figure 8). It is noted that, in general,

current GCMs are able to reasonably simulate large-scale atmospheric variables, such as SLP and Z500 (von Storch et al., 1993; Kang et al., 2004).

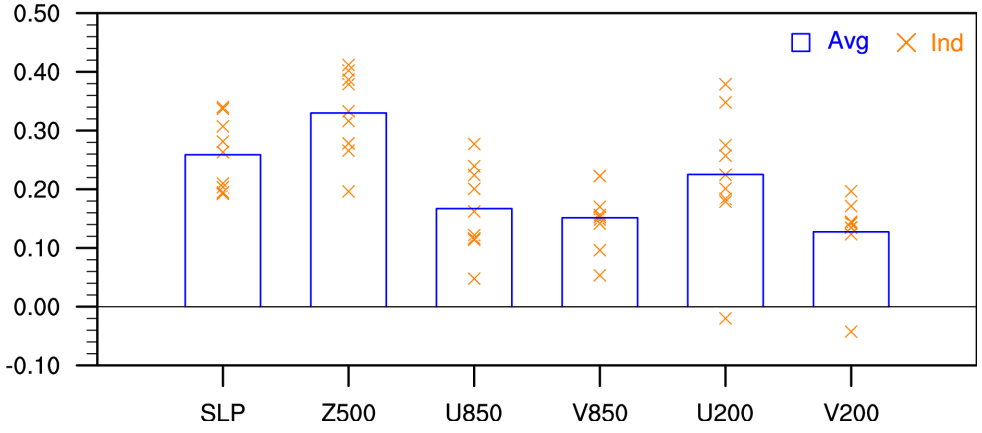


**Figure 9** TCCs between the observed and predicted December-May anomalous potential predictors, averaged over the predictor domain, during the 1983/84 to 2005/2006 period. Bars denote the average of the individual models' skills, and crosses denote single-model results.

Although temperature and precipitation predictions were substantially improved in the DMME when SLP and Z500 were used as predictors, the actual predictability did not reach the potential predictability of the perfect model. To investigate why the hybrid model has limitations in predicting station-scale variables, how the atmospheric large circulations from models are different from those of observations. Figure 10 shows EOF analyses of December to May anomalous SLP, based on observations and simulations for the first two EOF patterns and their respective PC time series. The first and second observed leading modes account for about 37% and 13% of the domain integrated variance, respectively. The first climate mode from observations is characterized by a meridionally dipole structure, with negative anomalies over the extratropics, and positive anomalies over the tropics. For the observed second mode, circulation features are zonally dipole compared with the first mode, and this is associated with the presence of a continental-scale high pressure system centered in Siberia, covering most of the Asian region.

There is broad agreement between the NCEP CFS simulated circulation and the observations. Compared to the observations, the pattern presented by NCEP CFS

is displaced slightly to the south for the first mode, and west for the second mode. However, the simulated SLP gradient is not as strong as the observed, and the patterns are difficult to reproduce in the PNU model simulations. There are also some deviations in terms of the strength and exact location of the maxima of the SLP field. It is of note that current GCMs suffer from some spatial drifts away from the observed climate (Palmer et al., 2004).

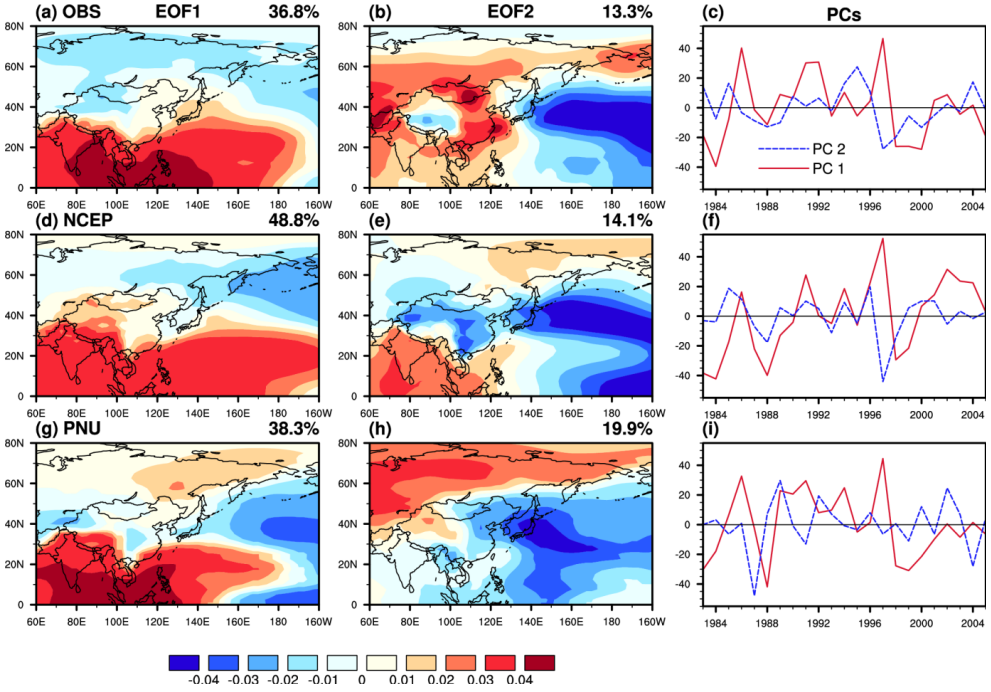


**Figure 10** EOF analyses of December-May anomalous SLP based on (a, b, c) observations, and simulations from (d, e, f) NCEP CFS, and (g, h, i) PNU for: (a, d, g) the first, and (b, e, h) the second EOF pattern, and (c, g, i) their respective PC time series. The fractional variance explained by each mode for the observations and model results are provided in the upper right of the panels in a, b, d, e, g, h.

## 3.3 Prediction and predictability of winter-to-spring drought

### 3.3.1 General skills for SPEI

We now assess the prediction skill and predictability for winter-to-spring droughts. The linear error in the probability score (LEPS) between the observed and predicted SPEI6 ending in May, are given in Figure 11. It can be seen that the error in the raw MME forecast is particularly large. A possible cause for this low skill could be attributed to the coarse resolution of the dynamical models used in this study, but it seems that model bias in the regional-scale circulation (Figure 10), such as the East Asian circulation response during ENSO, might play an even more important role (figure not shown). However, statistical downscaling is able to correct a large part of the systematic errors, even for forecasts with longer lead time (which can be clearly seen in Figures 11b and 11c).

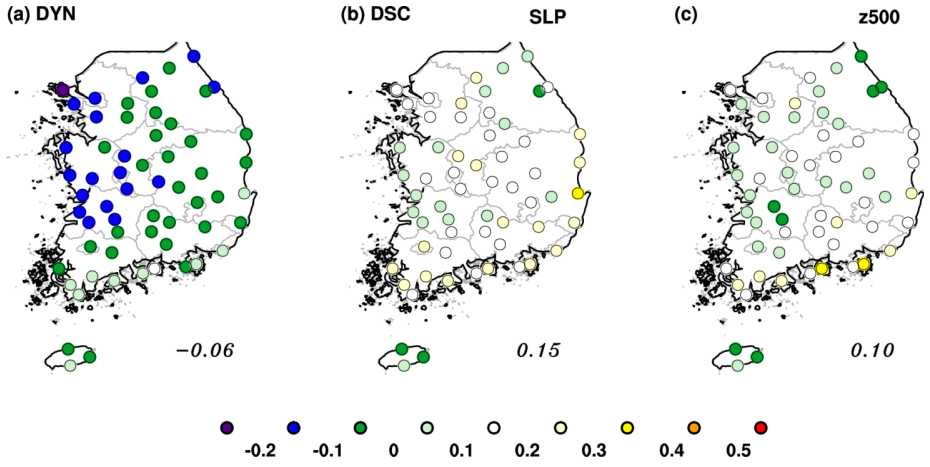


**Figure 11** The linear error in probability scores (LEPSs) between observations and predictions of: (a) raw MME; and (b, c) inflated DMME predictions with: (b) SLP, and (c) Z500 as the predictor, for SPEI6 from 1983/84 to 2005/06. The skill-score averaged over 60 station locations is given at the bottom right of each panel. Grey lines indicate the boundaries of the administrative areas in South Korea.

### 3.3.2 Skills for drought episodes

In order to compare the skills from the raw and downscaled MME during extreme episodes, the SPEI prediction skills are computed for selected extreme events[3]. From the results shown in Figure 12, it can be seen that the DMME has a generally better skill for predicting both drought and extreme flood events. The downscaling method in the present study was newly developed on the basis of a variant of the CCA, and can be used to understand the large-/regional-scale mechanisms controlling climate variability across the analyzed area, particularly with respect to extreme events (Busuioc et al., 2008). This CCA-based MOS method includes bias correction, and picks up climate signals from models that relate to station-scale variability. For this reason, it appears that DMME outperforms MME when it comes to extreme events such as floods and droughts, but for normal years the DMME demonstrated no better skill than the raw MME forecast.

3) The periods in which the absolute magnitude of observed December-May SPEI is greater than 0.5 (averaged over 60 station locations in South Korea) are chosen as dry events. These are the winter-to-spring periods of 1983/84, 1985/86, 1987/88, 1993/94, 1994/95, 1999/2000, and 2000/01 (7 dry episodes), and 1984/85, 1989/90, 1991/92, 1997/98, 2001/02, and 2002/03 (6 wet episodes). The rest 10 periods are normal cases

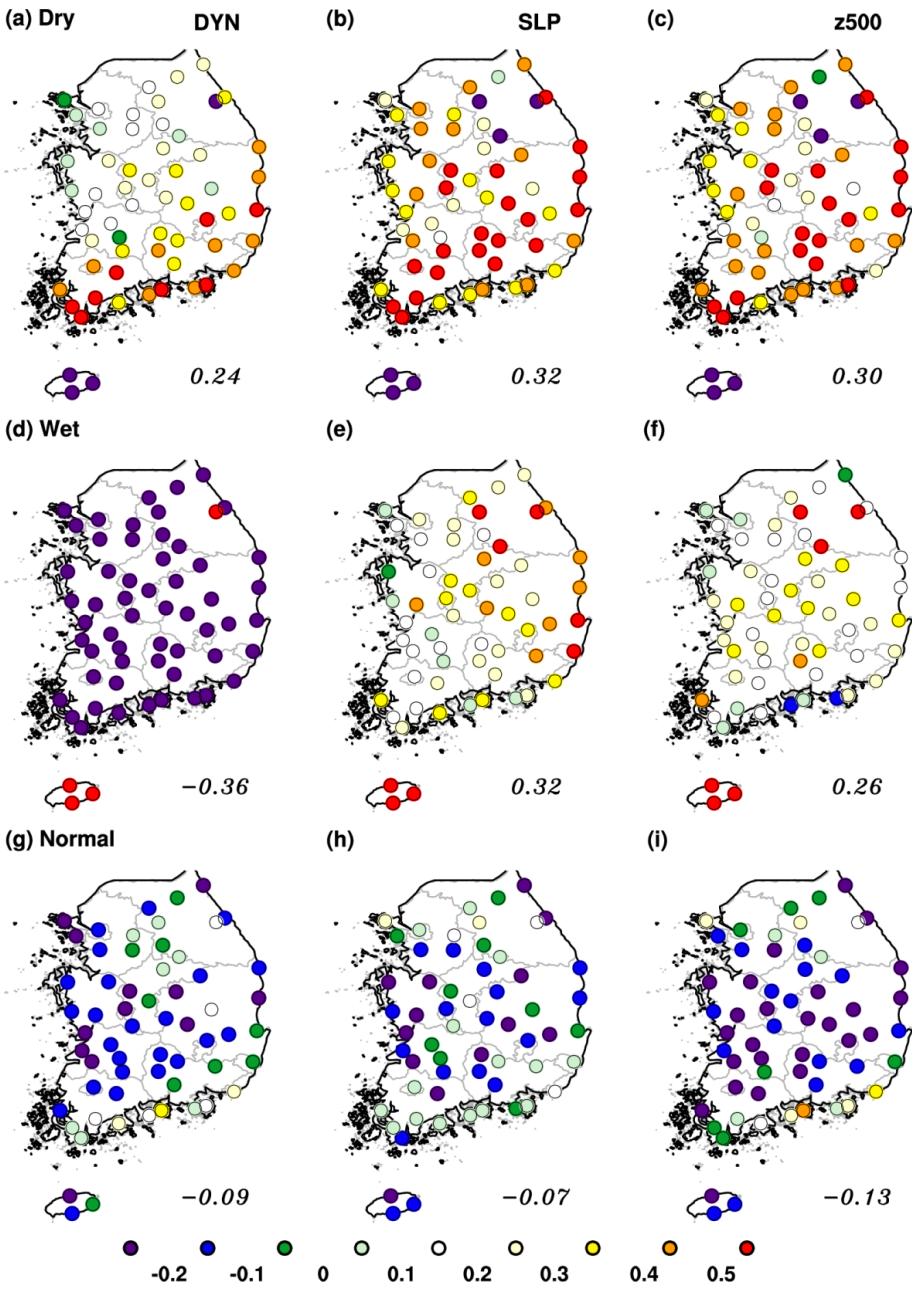


**Figure 12** The LEPSs between observations and predictions on: (a, d, g) raw MME; and (b, c, e, f, i) inflated DMME predictions with: (b, e, h) SLP; and (c, f, i) Z500 as predictors, for SPEI6 during: (a, b, c) dry, (d, e, f) wet, and (g, h, i) normal years. See text for details.

## 4. SUMMARY AND DISCISSION

Capturing climatic variation from boreal winter to spring is essential for the proper prediction of drought in South Korea. The variability and predictability of the South Korean climate during the period has been studied based on observed datasets and MME hindcast experiments archived at the APCC. A hydrological drought indicator, SPEI, depends on both precipitation and temperature, and can incorporate the effect of global warming using a balance between precipitation and evapotranspiration. The focus is on the leading modes of winter-to-spring variability over South Korea, which are identified based on multivariate EOF analysis of 6-month accumulated precipitation and surface air temperature. The first two leading climate modes, which account for about 80% of the total variance, are characterized by national-scale precipitation and temperature anomalies covering a whole region over South Korea.

A perfect empirical model was developed to reveal atmospheric dynamic linkage based on the observed datasets, and used as standard reference. The perfect model provides dynamically potential predictability of an empirical model, based on observed linkage. A new and novel hybrid dynamical-statistical method for predicting the December to May temperature and precipitation over South Korea was also developed and used in this study, and the potential of using the hybrid dynamical-statistical method for a 6 month-lead drought prediction was investigated. In particular, nine, one-tier climate models were statistically downscaled to predict the SPEI over 60 stations in South Korea. Bivariate downscaling was employed for both precipitation and temperature to maintain the physically coherent relation between them. This downscaling method was newly developed, and is based on a variant of CCA. It was evident that temperature and precipitation predictions were substantially improved in the DMME. However, due to their possible co-variability and its physical linkage to recurrent climate modes, such a statistical scheme in prediction the concatenated temperature and precipitation might not be the best performing scheme, out of various choices of schemes that are already available for those predicting station-scale temperature and precipitation, separately. The choice of most appropriate downscaling technique depends on the variables, seasons, regions of interest, on the availability of daily data, and whether the day to day correspondence of weather from the GCM needs

to be reproduced for some applications (Maurer and Hidalgo, 2008). Among other linear statistical downscaling methods, those based on CCA lead to a physical interpretation of the mechanism controlling regional climate variability (e.g. von Storch et al., 1993; Heyen et al., 1996, Busuioc et al., 2001; Tomozeiu et al., 2006) by selecting pairs of optimally correlated patterns between predictands and predictors.

The limitations, and reasons for the limitations, of the hybrid model were discussed in the current framework of dynamical climate prediction, and further improvement was considered. The same predictor domain was used for both an empirical perfect model and a hybrid model. This assumes that model can predict large-scale circulation patterns in time and space, since the domain was selected based on observed linkage in this study. Therefore, the hybrid model's skill for winter-to-spring precipitation and temperature mainly comes from its ability to capture an atmospheric large-scale circulation pattern in the dynamical models. However, due to the models' spatial biases, the actual predictability of the hybrid model is much lower than the potential predictability of the empirical perfect model. In other words, it appears that some (real) climate signal remains in the models, but it is displaced (see Figure 10). In order to consider the displacement of the predicted field from the observed climate, and to ensure a better performance from the downscaling forecast, a movable window (Kang et al., 2007; 2009) can be applied to this DMME method.

Finally, the results from such statistical downscaling applied to MME products (i.e. DMME) appears to outperform raw MME in capturing extreme floods and droughts (which is also evidence of the better performance in the LEP score from the former method), although it has to be said that the improvements of TCC at a station-scale from DMME (compared to raw MME) are only very marginal. Our results could lead to more reliable climatic extreme predictions for policymakers and stakeholders in the water management sector, and for better mitigation and climate adaptations.

## APPENDIX

### A1. Prediction equations

Decomposing predictor (Y), and predictand (T), into their truncated principal components gives:

$$Y(x,t) = \sum_{j=1}^{p} \kappa_j^{\frac{1}{2}} \alpha_j(t) e_j(x), \qquad x = 1, 2, \ldots, p,$$

$$T(x',t) = \sum_{j=1}^{q} \lambda_j^{\frac{1}{2}} \beta_j(t) f_j(x'), \; x' = 1, 2, \ldots, q. \quad \cdot \qquad \text{(A1)}$$

The separate sets of eigenvectors $e_j$ and $f_j$ are found in the usual manner and are orthonormal. In the following we use (p, q) to represent these truncation limits as appropriate. The variance and physical units are carried by the eigenvalues $\kappa_j$ and $\lambda_j$. The principal components $\alpha_j(t)$ and $\beta_j(t)$ are evaluated as follows. For $\alpha_j(t)$:

$$\alpha_j(t) = \sum_{x=1}^{p} Y(x,t)\, e_j(x), \; j = 1, 2, \ldots, p. \qquad \text{(A2)}$$

Similar calculations are performed for $\beta_j(t)$.

Optimal representation of T in terms of Y is obtained by first forming the set of all linear combinations of $\alpha_j$ and $\beta_j$ in the Euclidean vector space $E_n$:

$$u = \sum_{j=1}^{p} \alpha_j r_j \;\text{ and }\; v = \sum_{k=1}^{q} \beta_k s_k \qquad \text{(A3)}$$

where r and s are, by construction, arbitrary unit vectors in $E_p$ and $E_q$, respectively. For each choice of r and s define the correlation:

$$\langle u(t)v(t)\rangle_t = r^T C s \qquad \text{(A4)}$$

Where T denotes transpose and C is the p by q matrix whose elements are:

$$c_{jk} = \langle \alpha_j(t)\, \beta_j(t)\rangle_t. \qquad \text{(A5)}$$

It can be shown that the correlation of u and v in (A4) is maximized if r and s are, respectively, the eigenvectors of the systems:

$$\left.\begin{array}{ll}[CC^T]r_j = \mu_j^2 r_j & j = 1,2,\cdots,p \\ [C^T C]s_k = \mu_k^2 s_k & k = 1,2,\cdots,q\end{array}\right\} \quad \text{(A6)}$$

where $r_j=[r_{1j}, r_{2j}, \cdots, r_{pj}]^T$ and similarly for $S_k$. Matrix theory shows that the coefficient product matrices in (A6) have the same nonzero eigenvalues ($\mu^2$), and rank *l*=min[p, q], and that the $r_j$ and $s_k$ form orthogonal sets of vectors in $E_p$ and $E_q$, respectively. Remembering (A3), we obtain in this way the desired canonical component vectors:

$$u_j = \sum_{i=1}^{p} \alpha_i r_{ij} \text{ and } v_k = \sum_{i=1}^{q} \beta_i s_{ik}. \quad \text{(A7)}$$

The $u_j$ and $v_k$ each form orthonormal sets of vectors in $E_n$.

It follows at once from (A7) and the orthonormality of the $\alpha_j$ and $\beta_k$ that:

$$< \alpha_i(t)u_j(t) >_t = r_{ij} \text{ and } < \beta_j(t)v_k(t) >_t = s_{jk}. \quad \text{(A8)}$$

Moreover, by deriving (A6), we find for the case of q < p, that:

$$\left.\begin{array}{l}Cs_k = \mu_k r_k \\ C^T r_k = \mu_k s_k\end{array}\right\} \quad k=1, \cdots, q<p. \quad \text{(A9)}$$

The $\mu_j$ are the non-negative square roots of the eigenvalues $\mu_j^2$, j=1, ⋯, p, coming from the solutions of (A6). These may be arranged in descending order as follows:

$$\mu_1 = \cdots = \mu_s = 1 > \mu_{s+1} > \cdots > \mu_q > \mu_{q+1} = \cdots = \mu_p = 0 \quad \text{(A10)}$$

Where s = max[o, p + q - (n-1)]. In our work the truncated p and q are such that p + q <(n-1), so s = 0; hence the nondegenerate eigenvalues are $\mu_1^2, \cdots, \mu_q^2$. The remainder, namely, $\mu_j^2$, j = q + 1, ⋯, p, are zero.

From (A4), (A9), and (A10), it follows that:

$$< u_j(t)v_k(t) >_t = \begin{cases} \mu_k \delta_{jk} & j,k = 1,2,\cdots,q \\ 0 \quad j = q+1,\cdots,p; & k = 1,2,\cdots,q \end{cases} \quad \text{(A11)}$$

for the case q<p, which is the situation under study. Thus, the $\mu_j^2$ in (A6) are seen to be the squares of the correlation between $u_j$ and $v_j$ and the $\mu_j$ are called canonical correlation coefficients.

The above results allow us to represent the Y and T datasets as linear combinations of their canonical component vectors:

$$\left.\begin{array}{r} Y(x,t) = \sum_{j=1}^{p} \mathrm{u_j(t)} g_j(x) \\ \mathrm{T}(x',t) = \sum_{k=1}^{q} \mathrm{v_k(t)} h_k(x') \end{array}\right\} \qquad \text{(A12a)}$$

where we define:

$$\left.\begin{array}{l} g_j(x) = < Y(x,t)\mathrm{u_j(t)} >_{\mathrm{t}} \\ h_k(x') = < T(x',t)\mathrm{v_k(t)} >_{\mathrm{t}} \end{array}\right\} \quad . \qquad \text{(A12b)}$$

The canonical maps $g_j$ and $h_\kappa$ are vectors whose components show the correlation at a specific location ($x$ or $x'$) between Y or T and their respective canonical component time series (j or k). The $g_j$ and $h_\kappa$ maps as they are defined are not unit vectors, nor are they mutually orthogonal. It is convenient, for ease of interpretation, to deal with normalized versions of the g-maps. If these normalized maps are denoted by $g_j'$ then,

$$g_j'(x) = g_j(x) / \left\{ \sum_x \left[ g_j(x) \right]^2 \right\}^{1/2}$$

so that:

$$\sum_x \left[ g_j(x) \right]^2 \equiv 1 \ .$$

The cross correlations between, say, T and the $\mathrm{u_j}$ are, by (A11) and (A12):

$$< \mathrm{T}(x',t)\mathrm{u_j(t)} >_{\mathrm{t}} = \begin{cases} h_j(x')\mu_j & j = 1,2,\cdots,\mathrm{q} \\ 0 & j = q+1,\cdots,\mathrm{p} \end{cases} \qquad \text{(A13)}$$

For q<p and illustrate the weighting supplied by the canonical correlation coefficient $\mu_j$.

We wish to represent the n-dimensional predictand vector $T(x',.) = [T(x',1),\cdots, T(x',n)]^T$ by a linear combination of the canonical component vectors $\mathrm{u_j}$ of the predictor dataset. Geometrically, this is accomplished by recalling (A11) and then projecting the T vectors onto the q-dimensional vector space spanned by the first q of the $\mathrm{u_j}$; j=1, ⋯, q<p. This is achieved by first forming the n×n projection

matrix(additional information can be found in Barnett and Preisendorfer (1987):

$$P_u = \sum_{j=1}^{q} \mathrm{u_j} u_j^T$$

which has the properties:

$$P_u^T = P_u \text{ and } P_u = P_u P_u.$$

Then the least-squares estimate of T by Y is:

$$\hat{T}(x',\cdot) \equiv P_u T(x',\cdot)$$

i.e., by (A13):

$$\hat{T}(x',\cdot) = \sum_{j=1}^{q''} \mu_j \, \mathrm{u_j}(t) h_j(x')$$

$$x' = 1, \cdots, q'' \leq \mathrm{q}$$

$$\mathrm{t}=1, \cdots, \mathrm{n}. \qquad \text{(A14)}$$

## A2. Inflation

At time "*t*", the DMME prediction at a particular station "*k*", denoted by $Y_{(t,\ k)}$, is inflated to $Z_{(t,\ k)}$ according to the formula:

$$Z_{(t,k)} = Y_{(t,k)} \times IF_{(k)},$$

where $IF_{(k)}$ represent the inflation factor, $IF_{(k)} = \dfrac{\sigma_{OBS(k)}}{\sigma_{FCST(k)}}$ (Leung et al. 1999; Sohn et al. 2013a, 2013b). Among various inflation schemes, the method which simply rescales the variance of the predicted field to that based on climate records, irrespective of the prediction skill or the DMME variance itself at a particular station, gives the

best overall improvement in extreme drought and flood predictions (Sohn et al. 2013b).

## A3. Canonical map

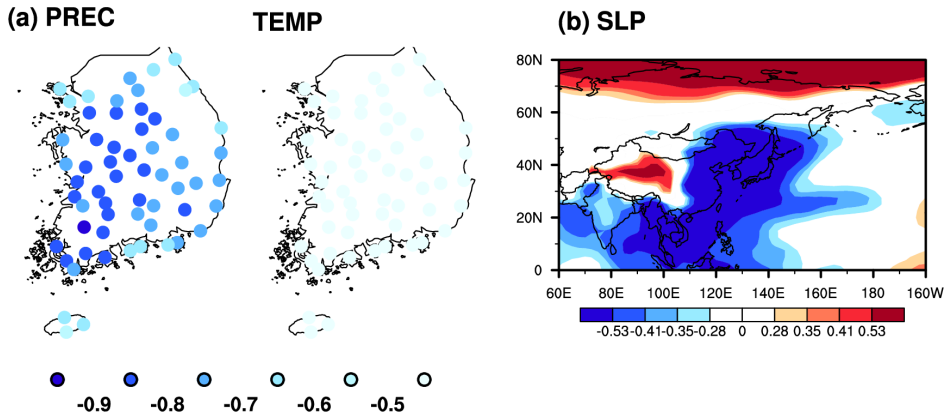


**Figure A1** Same as Figure 1 but for the second mode. These patterns explain 24% and 13% of the total variances for predictand and predictor, respectively. The correlation between the respective amplitude time series for these patterns is 0.62.

## REFERENCES


Acharya, N., N. A. Shrivastava, B. K. Panigrahi, and U. C. Mohanty, 2013: Development of an artificial neural network based multi-model ensemble to estimate the northeast monsoon rainfall over south peninsular India: an application of extreme learning machine, *Climate Dyn.*, DOI 10. 1007/s00382-013-1942-2.

Barlow, M., H. Cullen, B. Lyon, 2002: Drought in Central and Southwest Asia: La Niña, the Warm Pool, and Indian Ocean precipitation, *J. Climate*, 15, 697-700. doi: http://dx.doi.org/10.1175/1520-0442(2002)015 〈0697:DICASA〉 2.0.CO;2

Barnett, T., and R. Preisendorfer, 1987: Origins and levels of monthly and seasonal forecasts skill for United States surface air temperatures determined by canonical correlation analysis, *Mon. Wea. Rev.*, 115, 1825-1850.

Barnston, A. G., 1994: Linear statistical short-term climate predictive skill in the Northern Hemisphere, *J. Climate*, **7**, 1513-1564.

Barnston, A. G., and R. E. Livezey, 1987: Classification, seasonality and persistence of low-frequency atmospheric circulation pattern, *Mon. Wea. Rea.*, 115, 1083-1126.

Barnston, A. G., S. J. Mason, L. Goddard, D. G. Dewitt, and S. E. Zebiak, 2003: Multimodel ensembling in seasonal climate forecasting at IRI, *Bull. Am. Meteor. Soc.*, 84, 1783-1796.

Bretherton, C. S., C. Smith, and J. M. Wallace, 1992: An intercomparsion of method for finding coupled patterns in climate data, *J. Climate*, 5, 541-560.

Busuioc, A, D. Chen, and C. Hellström, 2001: Performance of statistical downscaling models in GCM validation and regional climate change estimates: Application for Swedish precipitation, *Int. J. Climatol.*, 21, 557-578.

Busuioc, A., R. Tomozeiu, and C. Cacciamani, 2008: Statistical downscaling model based on canonical correlation analysis for winter extreme precipitation events in the Emilia-Romagna region, *Int. J. Climatol.*, 28, 449-464. doi: 10.1002/jov.1547.

Busuioc, A., H. von Storch, and R. Schnur, 1999: Verification of GCM-generated regional seasonal precipitation for current climate and of statistical downscaling estimates under changing climate conditions, *J. Climate*, 12, 258-272.

Climate Test Bed, 2006, Multi-model ensembles: Transition from research to operations and implementation strategy, report, NOAA, Silver Spring, Md.

Cottrill, A., and Coauthors, 2013: Seasonal Forecasting in the Pacific Using the Coupled Model POAMA-2, *Wea. Forecasting*, 28, 668-680.

Doblas-Reyes, F. J., M. Deque, and J. P. Piedelievre, 2000: Multi-model spread and probabilistic seasonal forecasts in PROVOST, *Q. J. R. Meteor. Soc.*, 126, 2069-2088.

Doblas-Reyes, F. J., R. Hagedorn, and T. N. Palmer, 2005: The rationale behind the success of multi-model ensembles in seasonal forecasting-II. Calibration and combination, *Tellus*, 57A, 223-252.

Fu, X., and B. Wang, 2004: The boreal-summer intraseasonal oscillations simulated in a hybrid coupled atmosphere-ocean model, *Mon. Wea. Rev.*, 132, 2628-2649.

Gong, D. Y., and C. H. Ho, 2002: The Siberian high and climate change over middle to high latitude Asia, *Theor. Appl. Climatol.*, 72, 1-9.

Hagedorn, R., F. J. Doblas-Reyes, and T. N. Palmer, 2005: The rationale behind the success of multi-model ensembles in seasonal forecasting I. Basic concept, *Tellus*, 57A, 219-233.

Ham, Y. G., and I. S. Kang, 2010: Improvement of seasonal forecasts with inclusion of tropical instability waves on initial conditions, *Climate Dyn.*, 36, 1277-1290.

Ham, Y.-G., S. Schubert, and Y. Chang, 2012: Optimal initial perturbations for ensemble prediction of the Madden-Julian oscillation during boreal winter, *J. Climate*, 25, 4932-4945. doi: http://dx.doi.org/10.1175/JCLI-D-11-00344.1

Heyen, H., E. Zorita, and H. von Storch, 1996: Statistical downscaling of monthly mean North Atlantic air-pressure to sea level anomalies in the Baltic Sea, *Tellus*, 48A, 312-323.

Hoerling, M., and A. Kumar, 2003: The perfect ocean for drought, *Science*, 299, 691-694.

Jeong, H. I., and Coauthors, 2008: Experimental 6-month hindcast and forecast simulations using CCSM3, APCC 2008 Technical Report, APEC Climate Center.

Jhun, J.-G., and E.-J. Lee, 2004: A new East Asian winter monsoon index and associated characteristics of the winter monsoon, *J. Climate*, 17, 711-726.

Kalnay, E., M. Kanamitsu, R. Kistler, and Coauthors, 1996: The NCEP/NCAR 40-year reanalysis project, *Bull. Amer. Meteor. Soc.*, 77, 437-471.

Kang, H., K.-H. An, C.-K. Park, A. L. S. Solis, and K. Stitthichivapak, 2007: Multimodel output statistical downscaling prediction of precipitation in the Philippines and Thailand, *Geophys. Res. Lett.*, 34, L15710.

Kang, H., C.-K. Park, N. H. Saji, and K. Ashok, 2009: Statistical downscaling of precipitation in Korea using multimodel output variables as predictors, *Mon. Wea. Rev.*, 137, 1928-1938.

Kang, I.-S., J.-Y. Lee, and C.-K. Park, 2004: Potential predictability of summer mean precipitation in a dynamical seasonal prediction system with systematic error correction, *J. Climate*, 17, 834-844.

Kim, S., C.-K. Park, and M. K. Kim, 2005: The regime shift of northern hemisphere circulation responsible for the spring drought in Korea, *J. Korean Meteor. Soc.*, 41, 571-585.

Krishnamurti, T. N., C. M. Kishtawal, D. W. Shin, and C. E. Williford, 2000: Multi-model superensemble for weather and seasonal climate, *J. Climate.*, 13, 4196-4216.

Krishnamurti, T. N., C. M. Kishtawal, Z. Zhang, T. E. LaRow, D. R. Bachiochi, and Coauthors, 1999: Improved weather and seasonal climate forecasts from multi-model superensemble. *Science*, 285, 1548-1550.

Kug, J.-S., J.-Y. Lee, I.-S. Kang, B. Wang, and C.-K. Park, 2008: Optimal multi-model ensemble method in seasonal climate prediction, *Asia-Pacific J. Atms. Sci.*, 44, 233-247.

Lee, J. H., Y. H. Byun, and C.-K. Park, 2001: The characteristics of drought in the Korean Peninsula in the spring of 2001, *Atmosphere*, 11, 342-345 (in Korean).

Lee, J. Y., and Coauthors, 2010: How are seasonal prediction skills related to models' performance on mean state and annual cycle?, *Climate Dyn.*, 35, 267-283.

Lee, S. S., J. Y. Lee, K. J. Ha, B. Wang, and J. K. E. Schemm, 2011: Deficiencies and possibilities

for long-lead coupled climate prediction of the Western North Pacific-East Asian summer monsoon, *Climate Dyn.*, 36, 1173-1188.

Lee, W. J., and Cauthors, 2009: APEC 2009 final report, report, APEC Clim. Cent., Pusan, South Korea.

Leung, L. R. A. F. Hamlet, D. P. Lettenmarier, and A. Kumar, 1999: Simulations of the ENSO hydroclimate signals in the Pacific Northwest Columbia River Basin. *Bull. Am. Meteor. Soc.*, 80, 2313-2329.

Maurer, E. P., and H. G. Hidalgo, 2008: Utility of daily vs. monthly large-scale climate data: and intercomparison of two statistical downscaling methods, *Hydrol. Earth Syst. Sci.*, 12, 551-563.

McKee, T. B., N. J. Doesken, and J. Kleist, 1993: The relationship of drought frequency and duration to time scales, In Preprints of the 8th Conference on Applied Climatology, Anaheim, 179-184.

Merryfield, W. J., W. S. Lee, G. J. Boer, V. V. Kharin, J. F. Scinocca, G. M. Flato, R. S. AJayamohan, J. C. Fyfe, Y. Tang, and S. Polavarapu, 2013: The Canadian seasonal to interannual prediction system. Part I: Models and initialization, *Mon. Wea. Rev.*, 141, 2910-2945. Doi:10.1175/MWR-D-12-00216.1.

Michaelsen, J., 1987: Cross-validation in statistical climate forecast models, *J. Climate Appl. Meteor.*, 26, 1589-1600.

Min, S. K., W. T. Kwon, E. H. Park, Y. G. Choi, 2003: Spatial and temporal comparisons of droughts over Korea with East Asia, *Int. J. Climatol.*, 23, 223-233.

Min, Y.-M., V. N. Kryjov, K.-H. An, N. H. Saji, S.-J. Sohn, W.-J. Lee, and J.-H. Oh, 2011a: Evaluation of the weather generator CLIGEN with daily precipitation characteristics in Korea, *Asia-Pacific J. Atmos. Sci.*, 47, 255-263.

Min, Y.-M., V. N. Kryjov, and J.-H. Oh, 2011b: Probabilistic interpretation of regression-based downscaled seasonal ensemble predictions with the estimation of uncertainty, *J. Geophys. Res.*, 116, D08101, doi: 10.1029/2010JD015284.

Mu, Q., C. S. Jackson, and P. L. Stoffa, 2004: A multivariate empirical-orthogonal-function-based measure of climate model performance, *J. Geophys. Res.*, 109, D15101, doi:10.1029/2004JD004584.

Ogi, M., Y. Tachibana, and K. Yamazaki, 2003: Impact of the wintertime North Atlantic Oscillation (NAO) on the summertime atmospheric circulation, *Geophys. Res. Lett.*, 30(13), 1704, doi:10.1029/2003GL017280.

Palmer, T. N., A. Alessandri, U. Anderson, P. Cantelaube, M. Davey, and Cauthors, 2004: Development of a European multi-model ensemble system for seasonal to interannual prediction (DEMETER), *Bull. Am. Meteorol. Soc.*, 85, 853-872.

Palmer, T. N., C. Brankovic, and D. S. Richardson, 2000: A probability and decision-model analysis of PROBOST seasonal multi-model ensemble intergrations, *Q. J. R. Meteorol., Soc.*, 126, 2013-2034.

Park, C.-K., and S. D. Schubert, 1997: On the nature of the 1994 East Asian summer drought, *J. Climate*, 10, 1056-1070.

Potts, J. M., C. K. Folland, I. T. Jolliffe, and D. Sexton, 1996: Revised "LEPS" scores for assessing climate model simulations and long-range forecasts, *J. Climate*, 9, 34-53.

Saha, S., and Coauthors, 2010: The NCEP climate forecast system reanalysis, *Bull. Amer. Meteor. Soc.*, 91, 1015-1057. doi: 10.1175/2010BAMS3001.1

Schär, C., D. Lüthi, U. Beyerle, and E. Heise, 1999: The soil-precipitation feedback: a process study with a regional climate model, *J. Climate*, 12, 722-741.

Schubert, S., R. Koster, M. Hoerling, R. Seager, D. Lettenmaier, A. Kumear, and D. Gutzer, 2007: Predicting drought on seasonal-to-decadal time scales, *Bull. Am. Meteor. Soc.*, 88, 1625-1630.

Shukla, J., and Coauthors, 2000: Dynamical seasonal prediction, *Bull. Am. Meteor. Soc.*, 81, 2493-2606.

Sohn, S.-J., J.-B. Ahn, and C.-Y. Tam, 2013a: Six month-lead downscaling prediction of winter to spring drought in South Korea based on a multimodel ensemble, *Geophys. Res. Lett.*, 40, 579-583.

Sohn, S.-J., Y.-M. Min, J.-Y. Lee, C.-Y. Tam, I.-S. Kang, B. Wang, J.-B. Ahn, and T. Yamagata, 2012, Assessment of the long-lead probabilistic prediction for the Asian summer monsoon precipitation (1983-2011) based on the APCC multimodel system and a statistical model, *J. Geophys. Res.*, 117, D04102.

Sohn, S.-J., C.-Y. Tam, and J.-B. Ahn, 2011: Leading modes of East Asian winter climate variability and their predictability: An assessment of the APCC multi-model ensemble, *J. Meteor. Soc. Japan.*, 89, 455-474.

Sohn, S.-J., C.-Y. Tam, and J.-B. Ahn, 2013b: Development of a multimodel-based seasonal prediction system for extreme droughts and floods: a case study for South Korea, *Int. J. Climate*, 33, 793-805.

Sun, J. Q., and J. B. Ahn, 2011: A GCM-based forecasting model for the landfall of tropical cyclones in China, *Adv. Atmos. Sci.*, 28, 1049-1055.

Thompson, D. W., and J. M. Wallace, 2000: Annular modes in the extratropical circulation. Part I: Month-to-month variability, *J. Climate*, 13, 1000-1016.

Tomozeiu, C. Cacciamani, V. Pavan, A. Morgillo, and A. Busuioc, 2006: Climatic change scenarios of surface temperature in Emila-Romagna (Italy) obtained using statistical downscaling, Theoretical and Applied Climatology, doi: 10.107/s00704-0060275-z.

Tung, Y. L., C.-Y. Tam, S.-J. Sohn, and J. L. Chu, 2013: Improving the seasonal forecast for summertime South China rainfall using statistical downscaling, *J. Geophys. Res. Atmos.*, 118, 5147-5159, doi: 10.1002/jgrd.50367.

Vicente-Serrano, S. M., S. Begueria, and J. I. Lopez-Moreno, 2010, A multiscalar drought index sensitive to global warming: The Standardized Precipitation Evapotranspiration Index, *J. Climate*, 23, 1696-1718.

von Storch, H., E. Zorita, and U. Cubasch, 1993: Downscaling of global climate change estimates to regional scales: An application to Iberian rainfall in wintertime, *J. Climate*, 6, 1161-1171.

Wang, B., 1992: The vertical structure and development of the ENSO anomaly model during 1979-1989, *J. Atmos. Sci.*, 49, 668-712.

Wang, B., J. Y. Lee, I. S. Kang, J. Shukla, N. H. Saji, and C. K. Park, 2007: Coupled predictability of seasonal tropical precipitation, *CLIVAR Exchanges*, 12, 17-18.

Wang, B., J. Y. Lee, I. S. Kang, J. Shukla, J.-S. Kug, A. Kumar, J. Schemm, J.-J. Luo, T. Yamagata, C.-K. Park, 2008a: How accurately do coupled climate models predict the Asian-Australian monsoon interannual variability?, *Climate Dyn.*, 30, 605-619.

Wang, B., Z. Wu, J. Li, J. Liu, C. P. Chang, Y. Ding, and G. Wu, 2008b: How to measure the strength

of the east Asian summer monsoon?, *J. Climate*, 21, 4449-4463.

Wang, B., R. Wu, X. Fu, 2000: Pacific-East Asian Teleconnection: How does ENSO affect East Asia climate?, *J. Climate.*, 13, 1517-1534.

Wang, B., and Coauthors, 2009: Advance and prospectus of seasonal prediction: Assessment of the APCC/CliPAS 14-model ensemble retrospective seasonal prediction (1984-2004), *Climate Dyn.*, 33, 93-1117.

Wilks, D. S., 1995: Statistical Methods in the Atmosphere Science: An Introduction, Academic, San Diego, Calif.

Wood, A. W., E. P. Maurer, A. Kumar, and D. P. Lettenmaier, 2002: Long-range experimental hydrologic forecasting for the eastern United States, *J. Geophys. Res.*, 107, D20.

Yun, W. T., L. Stefanove, and T. N. Krishnamurti, 2003: Improvement of the superensemble technique for seasonal forecasts, *J. Climate*, 16, 3834-3840.

Yun, W. T., L. Stefanova, A. K. Mitra, V. V. Kumar, W. Dewar, and T. N. Krishnamurti, 2005: A multi-model superensemble algorithm for seasonal climate prediction using DEMETER forecasts, *Tellus*, 57A, 280-289.

## APCC RESEARCH REPORT 2013-02

- Construction of BSISO Forecast System and Application to Summer Monsoon Prediction
- Revision of Climate Change by Dynamic Downscaling over the Maritime Continents
- Long-Lead Station-Scaled Prediction of a Hydrological Drought in South Korea Based on Bivariate Downscaling
- Development of Scaled SVD Analysis and Related Methods with Focus on Application to Tropical-Extratropical Teleconnections

**APEC Climate Center**

12, Centum 7-ro, Haeundae-gu, Busan 612-020,
Republic of Korea
Tel: +82-51-745-3900 Fax: +82-51-745-3949
www.apcc21.org

비매품
94550
9 788997 333943
ISBN 978-89-97333-94-3
ISBN 978-89-97333-92-9 (세트)